THE JOURNAL OF PHYSICAL CHEMISTRY B

Article

Cite This: J. Phys. Chem. B 2018, 122, 6357−6363

pubs.acs.org/JPCB

Computational Investigation of the Effect of Backbone Chiral Inversions on Polypeptide Structure

Gül H. Zerze,[†] Mohammad Navaid Khan,[†,§] Frank H. Stillinger,[‡] and Pablo G. Debenedetti*[,†]

[†]Department of Chemical and Biomolecular Engineering and [‡]Department of Chemistry, Princeton University, Princeton, New Jersey 08544, United States

Supporting Information

ABSTRACT: Studying a set of helix-folding polyalanine peptides with systematically inserted chiral inversions in explicit water, we investigate quantitatively the effect of chiral perturbations on the structural ensembles of the peptides, thereby assessing the extent to which the backbone structure is able to fold in the presence of systematic heterochiral perturbations. Starting from the homochiral L-Ala_{20} peptide, we invert the backbone chiralities of Ala residues one by one along a specific perturbation pathway, until reaching the homochiral D-Ala_{20} peptide. Analysis of the helical contents of the simulated structural ensembles of the peptides shows that even a single inversion in the middle of the peptide completely breaks the helical structure in its vicinity and drastically reduces the helical content of the peptide. Further inversions in the middle of the peptide monotonically decrease the original helical content, that is, the right-handed helical content for L-Ala, and increase the helical content of the opposite chirality. Further analysis of the peptide ensembles using several size- and shape-related order parameters also indicate the drastic global changes in the peptide structure due to the local effects caused by the chiral inversions, such as formation of a reverse turn. However, the degree of the structural changes introduced by opposite chirality substitutions depends on the position of the inversion.

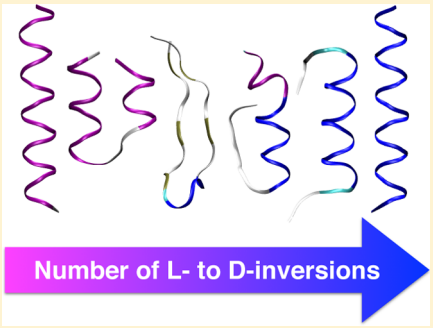

INTRODUCTION

The backbone of all proteinogenic amino acids except glycine contains an asymmetric tetrahedral α-carbon, the stereochemistry of which identifies the chirality of the corresponding amino acid as L- or D-amino acid. Although there are examples of naturally occurring D-amino acids, such as bacterial peptidoglycans as components of the bacterial cell wall,[1] antimicrobial peptides in microorganisms as well as in higher organisms,[2,3] free D-amino acids[4,5] or D-residue peptides in higher organisms including mammalian cells,[6−8] L-amino acids are by far the predominant enantiomer in all known life forms.

Homochirality is the hallmark feature of the chiral molecules of life, not only in the case of amino acids and the proteins they form by polymerization, but also in the monosaccharide components of nucleic acids, as well as the biologically important oligo- and polysaccharides, which are also almost exclusively homochiral.[9,10] The single-handedness of biomolecules is essential to their proper functioning; enzymatic specificity and molecular recognition rely on a particular enantiomer of the biomolecule. In the case of peptides, achieving correct folding is also ultimately tied to their appropriate functionality. The question thus naturally arises: can a protein or peptide tolerate any heterochirality and still achieve proper folding? What would be the degree of chiral inversion which significantly perturbs the structure of the peptide? Earlier experimental work showed evidence of structural perturbations by D-amino acids by studying the dimerization of helix-forming peptides,[11] which is in agreement with computational findings.[12] The degree of structural perturbation was shown to be dependent on the type of side chain of the inverted amino acid[13] as well as on the amino acid location.[14] Nanda and DeGrado[15] studied the simulated evolution of polyalanine chirality in the gas phase. They used a simplified energy function which only evaluates backbone hydrogen bonding, steric clashes described by a distance criterion, and the nonbonded interaction in a Monte Carlo sampling that allows chiral inversions in a given move. Their resulting ensemble showed that in order for sufficiently long peptides to form significant fractions of contiguous helices, homochiral conformers with terminal reversals must have higher weights, that is, they are the lower free energy structures. However, a microscopic investigation of the effect of systematic monomer-level chiral perturbations on peptide spatial architecture in aqueous solution has not been performed, and a study involving full atomistic detail, such as we perform in this work, has not been previously attempted.

Using a relatively simple, helix-folding peptide, we investigate the effect of systematic backbone chiral inversions on its structure. We perform exhaustive all-atom, solvent-explicit molecular dynamics (MD) simulations of 21 different 20-residue-long polyalanine peptides with different backbone chirality patterns. L- to D-inversions are systematically

Received: April 3, 2018
Revised: May 23, 2018
Published: May 24, 2018

DOI: 10.1021/acs.jpcb.8b03157
J. Phys. Chem. B 2018, 122, 6357−6363

Table 1. Amino Acid Composition of the Peptides Studied in This work[a]

Peptide	Sequence Composition (L-Ala/D-Ala)	# of L- to D-inversions
L-Ala$_{20}$	LLLLLLLLLLLLLLLLLLLL	0
L-Ala$_9$-D-Ala$_1$-L-Ala$_{10}$	LLLLLLLLLDLLLLLLLLLL	1
L-Ala$_9$-D-Ala$_2$-L-Ala$_9$	LLLLLLLLLDDLLLLLLLLL	2
L-Ala$_8$-D-Ala$_3$-L-Ala$_9$	LLLLLLLLDDDLLLLLLLLL	3
L-Ala$_8$-D-Ala$_4$-L-Ala$_8$	LLLLLLLLDDDDLLLLLLLL	4
L-Ala$_7$-D-Ala$_5$-L-Ala$_8$	LLLLLLLDDDDDLLLLLLLL	5
L-Ala$_7$-D-Ala$_6$-L-Ala$_7$	LLLLLLLDDDDDDLLLLLLL	6
L-Ala$_6$-D-Ala$_7$-L-Ala$_7$	LLLLLLDDDDDDDLLLLLLL	7
L-Ala$_6$-D-Ala$_8$-L-Ala$_6$	LLLLLLDDDDDDDDLLLLLL	8
L-Ala$_5$-D-Ala$_9$-L-Ala$_6$	LLLLLDDDDDDDDDLLLLLL	9
L-Ala$_5$-D-Ala$_{10}$-L-Ala$_5$	LLLLLDDDDDDDDDDLLLLL	10
L-Ala$_4$-D-Ala$_{11}$-L-Ala$_5$	LLLLDDDDDDDDDDDLLLLL	11
L-Ala$_4$-D-Ala$_{12}$-L-Ala$_4$	LLLLDDDDDDDDDDDDLLLL	12
L-Ala$_3$-D-Ala$_{13}$-L-Ala$_4$	LLLDDDDDDDDDDDDLLLL	13
L-Ala$_3$-D-Ala$_{14}$-L-Ala$_3$	LLLDDDDDDDDDDDDDLLL	14
L-Ala$_2$-D-Ala$_{15}$-L-Ala$_3$	LLDDDDDDDDDDDDDDLLL	15
L-Ala$_2$-D-Ala$_{16}$-L-Ala$_2$	LLDDDDDDDDDDDDDDDDLL	16
L-Ala$_1$-D-Ala$_{17}$-L-Ala$_2$	LDDDDDDDDDDDDDDDDDLL	17
L-Ala$_1$-D-Ala$_{18}$-L-Ala$_1$	LDDDDDDDDDDDDDDDDDDL	18
D-Ala$_{19}$-L-Ala$_1$	DDDDDDDDDDDDDDDDDDDL	19
D-Ala$_{20}$	DDDDDDDDDDDDDDDDDDDD	20

[a]All of the peptides are polyalanine peptides with different chiral compositions. L and D in the peptide sequences indicate L-alanine and D-alanine, respectively.

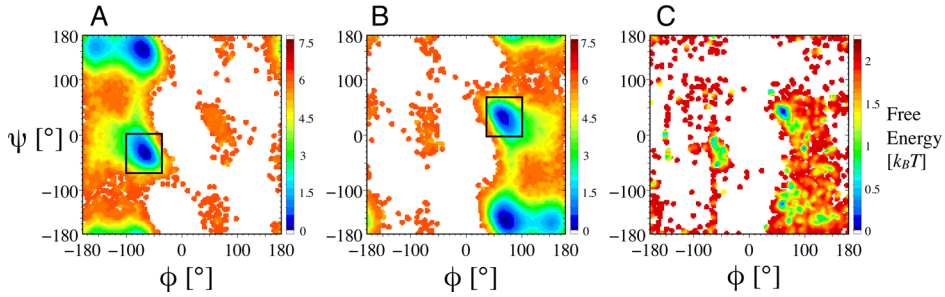

Figure 1. Free energy as a function of ϕ and ψ angles for L-Ala$_{20}$ (A) and D-Ala$_{20}$ (B) from simulations and for all D-amino acid occurrences (with a complete set of ϕ and ψ angles) in the Protein Data Bank as of 9/13/2017 (C). Identically sized black squares define the α_R (A) and α_L (B) regions used for the analysis in this study.

introduced from poly-L-alanine to poly-D-alanine, propagating the inversion from the middle residue. Analysis of the residual helix fraction shows that the local structure of the peptide is drastically perturbed, even with a single inversion, whereas the degree of perturbation in the total helical content is dependent on the position of the inversions. Further analysis of the peptides using the radius of gyration, end-to-end distance, and asphericity as order parameters also indicates drastic global changes in the peptide structure due to local perturbations caused by chiral inversions, and the degree of global changes is also found to be dependent on the position of the inversion.

METHODS

Inversion Pattern Design and Peptide Initial Configurations. Table 1 shows the primary structure of the 21 different 20-residue-long polyalanine peptides with a range of backbone chirality patterns. While the N- and C-terminal halves of the peptide's primary structure are symmetric for an even number of L- to D-inversions starting at the center, for odd numbers of perturbations, we always introduce L- to D-inversion on the N-terminus half.

Using an all-atom protein force field, the chirality of the asymmetric tetrahedral carbon atoms can be imposed as an initial condition for MD. The initial coordinates of the peptides with blocked ends are generated as extended structures using the CHARMM program[16] as Ace-L-Ala$_x$-D-Ala$_y$-L-Ala$_z$-Nme using the initial condition table of D-Ala from SwissParam,[17] where Ace and Nme refer to (N-terminal)-acetyl and (C-terminal)-*N*-methylamide groups, respectively. The initial extended structures are relaxed briefly in gas-phase simulations for 500 steps. Peptides are modeled using the Amber03w protein model[18] (see the Model subsection) and solvated in a truncated octahedron box of 3051 to 3070 TIP4P/2005 water molecules,[19] giving a system size of 12 416 to 12 492 atoms. Initial coordinates are energy-minimized and then equilibrated for 200 ps in the NVT ensemble followed by 200 ps in the NPT ensemble, where pressure is maintained at 1 bar using isotropic Berendsen pressure coupling[20] and temperature is maintained at 300 K using the Nosé–Hoover temperature coupling.[21,22]

Model. For the production simulations, we use the Amber03w protein force field and the TIP4P/2005 water model.[18,19] The only terms in the force field that have an intrinsic chirality are the dihedral angle terms. For example, the Ramachandran map [(ϕ,ψ) angles] of the peptide backbone with D-amino acids is rotated by 180° with respect to the corresponding map for a backbone composed of L-amino acids (Figure 1). All other terms in the force field are insensitive to chiral inversion. The dihedral angle terms with 0 or 180° phase shift angles also remain unaffected by chiral inversion. All dihedral potential terms in the Amber03w force field have phase shift angles of either 0 or 180°, that is, symmetric, except

DOI: 10.1021/acs.jpcb.8b03157
J. Phys. Chem. B 2018, 122, 6357–6363

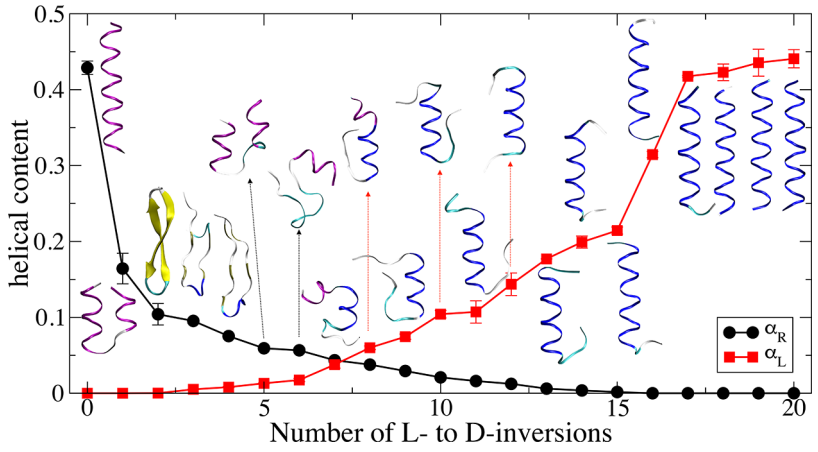

Figure 2. Average helical content of each polyalanine peptide. Errors are calculated as blocked standard errors using two equal, nonoverlapping blocks of data. The error bars are smaller than the symbol sizes for the data points not showing an error. The most populated structure of each peptide is also illustrated. Population percentages of the clusters are given in Table S1. Color coding of the structural elements is as follows; purple: right-handed helix, blue: left-handed helix, yellow: beta-sheet, cyan: turn, white: coil.

the backbone correction dihedral angle term, which has been introduced to recover secondary structure balance.[18,23] To address this asymmetry, we create modified residue topology entries for D-amino acids, using the inverted phase shift angle for the dihedral potential term associated with the backbone correction. We simulate our systems using the GROMACS 2016.3[24,25] MD engine and PLUMED 2.3.1 for metadynamics calculations.[26] The D-alanine entry of the GROMACS-compatible Amber03w force field file for residue topology is given in the Supporting Information.

Parallel Tempering in Well-Tempered Ensembles. To ensure the equilibrium sampling of each peptide in aqueous solution, we perform parallel tempering in well-tempered ensemble (PTWTE) simulations[27−29] of the peptides for at least 300 ns/replica. Convergence is monitored by the average helical content as a function of time for a 300 K replica of each peptide (Figures S1 and S2). The initial 100 ns/replicas are treated as equilibration and excluded from the analysis for all peptides.

PT[27] is a well-established enhanced sampling technique where multiple copies, replicas, of the system are run in parallel at different temperatures and exchanges between adjacent temperatures are attempted periodically. However, the PT method suffers from the scaling behavior of the number of required replicas with the system size to attain a reasonable exchange acceptance ratio. A recently introduced metadynamics-based technique, WTE,[28] alleviates this issue by amplifying potential energy fluctuations, while maintaining the same potential energy average. The combined method, PTWTE has been shown to significantly reduce the number of replicas.[28,29] In this work, we use PTWTE where the potential energy is biased using 500 kJ/mol Gaussian width, 1.0 kJ/mol initial Gaussian height, with Gaussian potentials added every 2000 steps, with a bias factor of 20. Prior to starting the PTWTE simulations, unbiased simulations at each replica temperature are performed for 200 ps to equilibrate the potential energy of the replicas. Temperatures of the 14 replicas are distributed geometrically spanning a range of 300−475 K. The average replica exchange acceptance ratio is 35%. All runs are performed in the NPT ensemble.

Systems are propagated using the leap-frog algorithm with a 2 fs time step. The temperature of each replica is maintained using the Nosé−Hoover thermostat[21,22] with a 1 ps time constant. The pressure of each replica is maintained at 1 bar using a Parrinello−Rahman barostat with an isotropic coupling with a time constant of 2 ps. Electrostatic interactions are calculated using the particle-mesh Ewald method[30] with a real space cutoff distance of 0.9 nm. A 1.2 nm cutoff distance is used for the van der Waals interactions.

Analysis. The helical content of the peptides is calculated as the ratio of the total number of helical blocks to the maximum possible number of helical blocks.[31−33] First, a helix or a coil state is assigned to each residue for each configuration, based on the block definition as follows. A right-handed α-helical block is defined if any 3 consecutive residues are in the α_R basin of the Ramachandran map. Similarly, a left-handed α-helical block is assigned when any 3 consecutive residues of the peptide are in the α_L basin of the Ramachandran map. The (ϕ,ψ) boundaries of α_R and α_L basins are defined as α_R: $-100° \leq \phi \leq -30°$, $-70° \leq \psi \leq 0°$ and α_L: $30° \leq \phi \leq 100°$, $0° \leq \psi \leq 70°$, as shown in Figure 1. The states of residues that do not satisfy the above-described α_L or α_R criteria are assigned to be coil. Once the state of each residue is assigned as helix or coil, the helical content of a configuration is evaluated as the ratio of the total number of 3 consecutive-residue blocks in the helix state to the maximum possible number blocks of the same length, which is 18 for a three residue-long block criterion and a 20 residue-long peptide. The average over all configurations defines the average helical content of the peptide.

Similarly, a fraction of per-residue helices are also calculated by assigning the state of each residue to an α_R, α_L, or coil for each configuration based on the above-described criteria. Then, for each residue, a fraction of α_R and α_L are defined as the ratio of the number of configurations in the α_R and α_L state, respectively, to the total number of configurations.

Clustering is performed based on structural similarity of the backbone-heavy, that is, nonhydrogen, atoms following the GROMOS algorithm[34] using a 0.30 nm root mean square deviation (rmsd) cutoff distance. Helix maps showing the α_R or α_L propensities as a function of residue interval and the helix length are calculated following the ss-map algorithm by Iglesias et al.[35] using the same ϕ, ψ boundaries defined above. Asphericity is calculated using the following expression: 1/

DOI: 10.1021/acs.jpcb.8b03157
J. Phys. Chem. B 2018, 122, 6357−6363

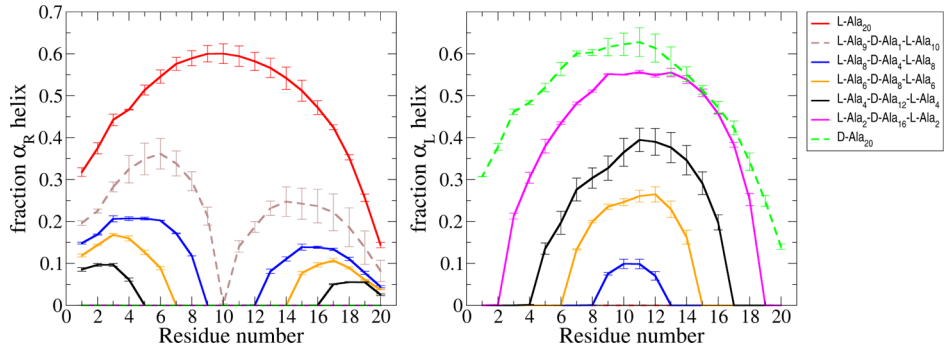

Figure 3. Fraction of right-handed (left) and left-handed (right) helices per-residue. Results for seven peptides are shown here for clarity. All inclusive plot is shown in Figure S3. Errors are calculated as blocked standard errors using two equal, nonoverlapping blocks of data.

$2(\sum_{i>j=1}^{3}(R_i^2 - R_j^2)^2)/(\sum_{i=1}^{3}(R_i^2))$, where the R_i is the principal radii of gyration calculated using backbone-heavy atoms.

RESULTS AND DISCUSSION

α-Helices are the most prevalent structural elements in proteins, and they are stabilized by the backbone hydrogen bonds between residues i and $i + 4$ (or residues i and $i + 3$ for shorter 3_{10} helices[36]). The conformational landscape of an α-helical peptide typically involves nonhelical and partially or fully helical conformers with comparable free energies. In this work, we characterize the helical content of the peptides as the ratio of the total number of helical blocks to the maximum possible number of helical blocks (see the Analysis subsection of the Methods). Figure 2 shows the average helical content of each polyalanine peptide, including both right-handed α-helices (α_R) and left-handed α-helices (α_L), as a function of the number of amino acids inverted from L-enantiomer to D-enantiomer, along with a representative structure of the most populated cluster of each peptide. The percentages of the three most populated clusters, which provide a measure of structural heterogeneity in each peptide, are tabulated in Table S1. Because we study 20-residue-long polyalanine peptides, the numbers "0" and "20" L- to D-inversions represent poly-L-alanine and poly-D-peptides, respectively. Steric effects arising from hindrance between the backbone carbonyl and the side-chain moiety make negative ϕ angles ($-180° < \phi < 0°$) energetically more favorable for the backbone of L-amino acids. For the opposite chirality, D-amino acids, the opposite is the case, and, positive ϕ angles are more favorable by an identical amount, as shown Figure 1 [(A,B) simulation results and (C) protein data bank analysis for D-amino acids)]. This symmetry was shown to hold for all amino acids in a simulation study of a glycine-based host−guest pentapeptide system (GGXGG) as well.[37] As expected from the above-described steric effects, the poly-L-alanine peptide forms exclusively right-handed α-helical (α_R) structures, whereas the poly-D-alanine peptide forms exclusively α_L helices with a fraction identical to that of α_R for poly-L-alanine (Figure 2). This is consistent with our expectation that the potential energy function is invariant to chiral inversion. An M06/6-311G(d,p) level quantum mechanical study also showed that the right-handed helix configuration of poly-L-alanine and the left-handed helix configuration of the same length poly-D-alanine are equally favorable energetically, both in vacuo and in water,[38] supporting our molecular mechanical approach.

An important asymmetry factor in the design of this study is that it can show how the position of the chiral inversion can affect the structure. Each L- to D-inversion involves a D-alanine introduced in the central region of the peptide. This design results in a central block of D-alanines with flanking blocks of L-alanines. Therefore, the calculations are designed to compare and contrast L- to D-inversions in the middle of the peptide with D- to L-inversions in the peptide's flanking (terminal) regions. In contrast to the sharp decrease in the α_R content of the peptide with a single centrally located L- to D-inversion, the α_L content does not show a similarly sharp decrease with a single terminally located D- to L-inversion (Figure 2). Rather, it shows an approximately constant total helical content for the first few (n = 1, 2, 3) D- to L-inversions ($20 - n$ L- to D-inversions), within statistical noise. This implies that the total helical content is more robust to chiral inversion in the flanking regions of the peptide.

The per-residue α_R fraction of the L-Ala$_{20}$ peptide is the same as the corresponding per-residue α_L fraction of the D-Ala$_{20}$ peptide within statistical noise (Figure 3). With a single L- to D-inversion in the middle, the α_R fraction in the middle of the peptide is completely suppressed (Figure 3, left panel).

After the third L- to D-inversion, the α_L fraction per residue starts to be visible (Figure 3, right panel and Figure S3, right panel). Given that the required minimum length is 3 for a helical block to occur according to our definition, α_L helices start to appear as immediately as possible. As the number of adjacent D-amino acids increases in the middle of the peptide, the α_L fraction also increases over the region encompassing D-amino acids.

As the third level of helical analysis, we calculate the right-handed (Figure 4) and the left-handed (Figure 5) helix maps of the peptides. These maps are capable of showing the composition of the partial helical configurations sampled by each peptide, according to the length (x-axis) of the helix and the residue interval involving that particular helical block (y-axis). Each residue of each frame is assigned to the α_R or α_L state if they satisfy the (ϕ,ψ) angle criteria that we provide in the Methods section. Then, they are normalized for the total number of frames in the trajectory. For the total helical content analysis (Figure 2), a block is defined as α-helix if three consecutive residues are in the α-helix basin (Figure 1). Accordingly, structure lengths of 1 and 2 in these maps (Figures 4 and 5) do not contribute to the helical content of the peptides, but they still provide useful information as they show the propensity of being in the α_R or α_L basin, regardless of whether the residue is in a helical block or not. Per-residue summation of the propensities over helix length for lengths ≥ 3 yields the helix fraction per-residue, as given in Figure 3.

The severe impact of the first L- to D-inversion is clearly shown in Figure 4. As opposed to the poly-L-alanine peptide

DOI: 10.1021/acs.jpcb.8b03157
J. Phys. Chem. B 2018, 122, 6357−6363

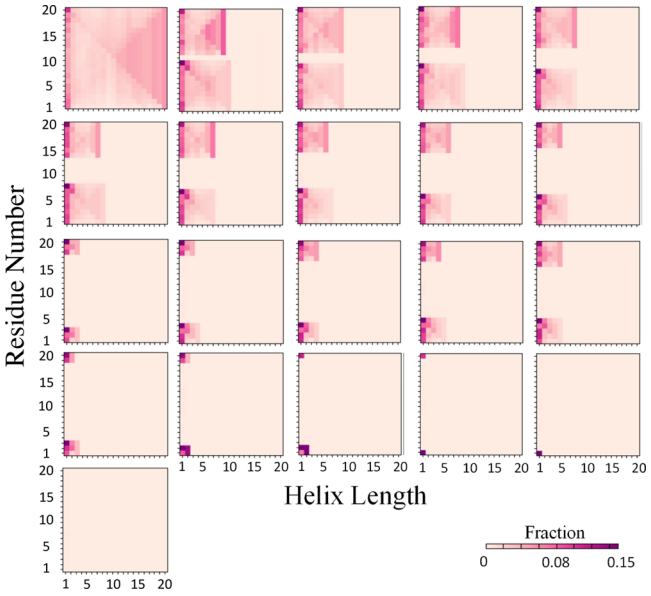

Figure 4. α_R propensities as a function of length and residue interval for each peptide. Panels are organized according to the number of L- to D-inversions in the peptides whose sequences are shown in the Table 1. The top left corner represents the peptide with 0 L- to D-inversions. From left to right, the number of L- to D-inversions increases by one and continues from the left-most column of the next row.

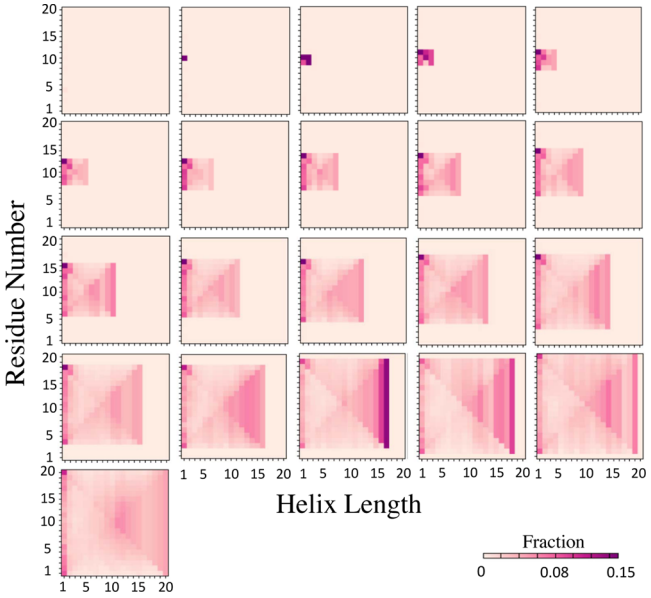

Figure 5. α_L propensities as a function of length and residue interval for each peptide. Panels are organized according to the number of L- to D-inversions in the peptides whose sequences are shown in the Table 1. The top left corner represents the peptide with 0 L- to D-inversions. From left to right, the number of L- to D-inversions increases by one and continues from the left-most column of the next row.

which can sample the entire range of helical blocks from lengths 1 to 20, the singly mutated peptide is not able to sample contiguous helical segments longer than 10. As the number of inversions increases, the non-α_R segment in the middle spans a larger residue interval and the α_R-helical segments become shorter. On the other hand, there is a significant α_L fraction at the inversion point by the first L- to D-inversion (Figure 5, second panel from the left in the top row). As the number of L- to D-inversions increases, the α_L-helical segments elongate, and once the peptide becomes poly-D-alanine (i.e., all 20 positions inverted), the α_L-helix map (Figure 5, last row panel) becomes the same as the α_R-helix map of poly-L-alanine (Figure 4, first panel from the left in the top row).

Looking at the sampling of individual residues, regardless of whether they are in a helical block of three consecutive residues or not, the L-Ala_9-D-Ala-L-Ala_{10} peptide demonstrates that the D-alanine in the middle practically does not sample the α_R basin of the Ramachandran map (Figure 4, second panel from the left in the top row). Rather, it predominantly samples the α_L basin (Figure 5, second panel from the left in the top row). Therefore, it causes a break of long right-handed helices in the middle of the peptide. Considering the opposite inversions, that is, D- to L-inversions from the terminal sides toward the middle, a singly mutated peptide also loses its ability to sample the α_R basin. However, because of its position, such a mutation does not break relatively longer helical segments. It is clear from the helix maps that any D-Ala, independent of the position or the neighbors, always samples the α_L basin, whereas any L-Ala always samples the α_R basin.

We also test the ability of the peptide to form i, $i + 4$ hydrogen bonds if it can assume an appropriate configuration defined by backbone torsional angles. We create a conformer with all $\phi = -57°$, $\psi = -47°$, torsional angles for an ideal right-handed helix, both for L-Ala_9-D-Ala-L-Ala_{10} and L-Ala_{20} peptides. A hydrogen bond-based secondary structure analysis (DSSP[36]) indicates that all hydrogen bonds necessary for a right-handed helix are formed in this configuration (Figure S4) for both peptides. This analysis confirms that the peptide would be able to form the necessary hydrogen bonds for a long helix if it is able to locate such a conformer through conformational exploration. However, these conformations have a higher energy for L-Ala_9-D-Ala-L-Ala_{10} compared to L-Ala_{20}, as shown in Figure S4. This is due to excluded volume interactions between side chains and carbonyl moieties, restricting the sampling for the required right-handed helix. We do not find such configurations in L-Ala_9-D-Ala-L-Ala_{10} in explicit water, whereas similar conformers (within 0.3 nm rmsd) form the most populated cluster of L-Ala_{20} (see the snapshot in the top left corner of Figure 2). The effect of a small number of inversions is more drastic in the middle because of broken cooperativity; the total helical fraction for one large helix is greater than the helical fraction corresponding to two short segments for the same number of inversions and the peptide length.

We further characterize the peptide structure using the right-handed/left-handed helical content and a peptide size-related order parameter, the radius of gyration (R_g). Figure 6 shows the free energy surface of the peptide as a function of right-handed/left-handed helical content and R_g at 300 K. The helical content coordinate is the same quantity whose average is shown in Figure 2. There are two distinct free energy basins for L-Ala_{20} and the peptides whose number of L- to D-inversions is equal to or greater than 14. One is nonhelical, the other is a highly helical state, with helical content close to 1. The nonhelical basin is the only low free energy basin for all remaining peptides. The nonhelical basin shows differences between the peptides. While the nonhelical basin of poly-L-alanine is centered around an R_g of 1.25 nm, the center is shifted toward a smaller R_g, 0.8−0.9 nm, for 10 of the peptides with $1 \leq$ L- to D-inversions ≤ 11, indicating a larger population of more compact, nonhelical structures for these peptides. As can be

DOI: 10.1021/acs.jpcb.8b03157
J. Phys. Chem. B 2018, 122, 6357−6363

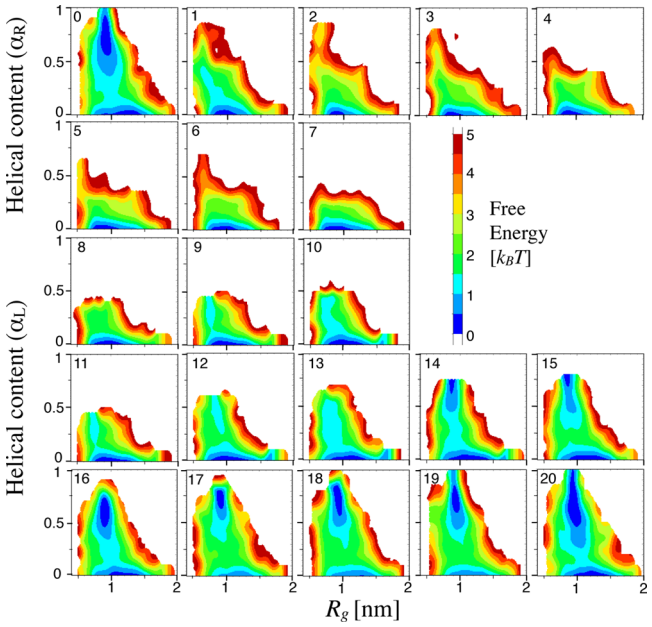

Figure 6. Free energy surface of the polyalanine peptides at 300 K as a function of radius of gyration, R_g, and right- or left-handed helical content. Numbers on the upper right corner of each panel indicate the number of L- to D-inversions. α_R content is used up to 7 L- to D-inversions, and α_L is used for the remaining peptides, as they are the dominant helical form observed in the peptides of given composition.

visualized by the change in the most populated cluster of these peptides (Figure 2, overlaid snapshots), there is a compactness introduced by a reverse turn as a result of opposite chirality substitutions in the middle. The sharp change in the peptide's size by the first L- to D-inversion is also shown clearly by the average R_g as a function of the number of L- to D-inversion (Figure S5). For the peptides with a number of L- to D-inversions >13, the opposite chirality helix dominates the structure and, accordingly, the second basin, a highly helical state, reappears (Figure 6). Similar observations are also made using other parameters: end-to-end distance (Figure S6) and asphericity (Figure S7).

CONCLUSIONS

Studying a systematically L- to D-mutated polyalanine peptide via enhanced-sampling atomistic simulations, we quantitatively assess the effect of chiral perturbations on a helix-folding peptide using a rigorous analysis of helical content, as well as other order parameters. Although it is intuitive to think that replacement of an L-amino acid with a D-amino acid will affect the peptide backbone because of the corresponding opposite steric effects, the observation of a peptide backbone showing no tolerance to even a single inversion in its middle section is remarkable. There are cases in nature where L-amino acids can predominantly sample the α_L region of the Ramachandran map, for example, the beta-turn elements that are found in the hairpin-like structures of proteins.[39,40] This indicates that despite unfavorable steric constraints, L-amino acids are still capable of sampling the α_L region, which is in agreement with computational results.[41]

Although there is no consensus as to how biomolecular homochirality emerged in prebiotic Earth, our findings suggest that it can be essential in order for α-helical segments to achieve their correct folding. For a simple helix-folding peptide, we show that arbitrary heterochirality is not tolerable if the peptide is to maintain its native structure. Chiral inversions cause a significant change in the local structure, and depending on the location of the inversion, they can also cause global changes in the peptide structure, which conspire against folding into the native structure.

ASSOCIATED CONTENT

Supporting Information

The Supporting Information is available free of charge on the ACS Publications website at DOI: 10.1021/acs.jpcb.8b03157.

GROMACS-compatible residue topology (.rtp) entry for D-Ala residue (PDF)

AUTHOR INFORMATION

Corresponding Author

*E-mail: pdebene@princeton.edu.

ORCID

Gül H. Zerze: 0000-0002-3074-3521

Frank H. Stillinger: 0000-0002-1225-8186

Pablo G. Debenedetti: 0000-0003-1881-1728

Present Address

§2501 NE Century Blvd Hillsboro, OR 97124, USA.

Notes

The authors declare no competing financial interest.

ACKNOWLEDGMENTS

Computations of this work were performed at the Terascale Infrastructure for Groundbreaking Research in Science and Engineering (TIGRESS) High Performance Computing Center. G.H.Z., M.N.K., and P.G.D. thank Unilever Research and Development for funding.

REFERENCES

(1) Lam, H.; Oh, D.-C.; Cava, F.; Takacs, C. N.; Clardy, J.; de Pedro, M. A.; Waldor, M. K. D-amino acids govern stationary phase cell wall remodeling in bacteria. *Science* **2009**, *325*, 1552−1555.

(2) Gevers, W.; Kleinkauf, H.; Lipmann, F. Peptidyl transfers in gramicidin S biosynthesis from enzyme-bound thioester intermediates. *Proc. Natl. Acad. Sci. U.S.A.* **1969**, *63*, 1335−1342.

(3) Kreil, G. D-amino acids in animal peptides. *Annu. Rev. Biochem.* **1997**, *66*, 337−345.

(4) Dunlop, D. S.; Neidle, A.; McHale, D.; Dunlop, D. M.; Lajtha, A. The presence of free D-aspartic acid in rodents and man. *Biochem. Biophys. Res. Commun.* **1986**, *141*, 27−32.

(5) Hashimoto, A.; Kumashiro, S.; Nishikawa, T.; Oka, T.; Takahashi, K.; Mito, T.; Takashima, S.; Doi, N.; Mizutani, Y.; Yamazaki, T.; Kaneko, T.; Ootomo, E. Embryonic development and postnatal changes in free D-aspartate and D-serine in the human prefrontal cortex. *J. Neurochem.* **1993**, *61*, 348−351.

(6) Fujii, N.; Saito, T. Homochirality and life. *Chem. Rec.* **2004**, *4*, 267−278.

(7) Helfman, P. M.; Bada, J. L. Aspartic acid racemization in tooth enamel from living humans. *Proc. Natl. Acad. Sci. U.S.A.* **1975**, *72*, 2891−2894.

(8) Bada, J. L. In Vivo racemization in mammalian proteins. *Methods Enzymol.* **1984**, *106*, 98−115.

(9) Blackmond, D. G. The origin of biological homochirality. *Cold Spring Harbor Perspect. Biol.* **2010**, *2*, a002147.

(10) Bonner, W. A. The origin and amplification of biomolecular chirality. *Origins Life Evol. Biospheres* **1991**, *21*, 59−111.

(11) Fairman, R.; Anthony-Cahill, S. J.; DeGrado, W. F. The helix-forming propensity of D-alanine in a right-handed α-helix. *J. Am. Chem. Soc.* **1992**, *114*, 5458−5459.

DOI: 10.1021/acs.jpcb.8b03157
J. Phys. Chem. B 2018, 122, 6357−6363

(12) Hermans, J.; Anderson, A. G.; Yun, R. H. Differential helix propensity of small apolar side chains studied by molecular dynamics simulations. *Biochemistry* **1992**, *31*, 5646−5653.
(13) Krause, E.; Bienert, M.; Schmieder, P.; Wenschuh, H. The helix-destabilizing propensity scale of D-amino acids: the influence of side chain steric effects. *J. Am. Chem. Soc.* **2000**, *122*, 4865−4870.
(14) Krause, E.; Beyermann, M.; Dathe, M.; Rothemund, S.; Bienert, M. Location of an amphipathic α-helix in peptides using reversed-phase HPLC retention behavior of D-amino acid Analogs. *Anal. Chem.* **1995**, *67*, 252−258.
(15) Nanda, V.; DeGrado, W. F. Simulated evolution of emergent chiral structures in polyalanine. *J. Am. Chem. Soc.* **2004**, *126*, 14459−14467.
(16) Brooks, B. R.; Brooks, C. L.; Mackerell, A. D.; Nilsson, L.; Petrella, R. J.; Roux, B.; Won, Y.; Archontis, G.; Bartels, C.; Boresch, S.; Caflisch, A.; et al. CHARMM: the biomolecular simulation program. *J. Comput. Chem.* **2009**, *30*, 1545−1614.
(17) Gfeller, D.; Michielin, O.; Zoete, V. SwissSidechain: a molecular and structural database of non-natural sidechains. *Nucleic Acids Res.* **2012**, *41*, D327−D332.
(18) Best, R. B.; Mittal, J. Protein simulations with an optimized water model: cooperative helix formation and temperature-induced unfolded state collapse. *J. Phys. Chem. B* **2010**, *114*, 14916−14923.
(19) Abascal, J. L. F.; Vega, C. A general purpose model for the condensed phases of water: TIP4P/2005. *J. Chem. Phys.* **2005**, *123*, 234505.
(20) Berendsen, H. J. C.; Postma, J. P. M.; van Gunsteren, W. F.; DiNola, A.; Haak, J. R. Molecular dynamics with coupling to an external bath. *J. Chem. Phys.* **1984**, *81*, 3684−3690.
(21) Nosé, S. A dynamics method for simulations in the canonical ensemble. *Mol. Phys.* **1984**, *52*, 255−268.
(22) Hoover, W. G. Canonical dynamics: equilibrium phase-space distributions. *Phys. Rev. A: At., Mol., Opt. Phys.* **1985**, *31*, 1695.
(23) Best, R. B.; Hummer, G. Optimized molecular dynamics force fields applied to the helix-coil transition of polypeptides. *J. Phys. Chem. B* **2009**, *113*, 9004−9015.
(24) Berendsen, H. J. C.; van der Spoel, D.; van Drunen, R. GROMACS: A message-passing parallel molecular dynamics implementation. *Comput. Phys. Commun.* **1995**, *91*, 43−56.
(25) Hess, B.; Kutzner, C.; Van Der Spoel, D.; Lindahl, E. GROMACS 4: Algorithms for highly efficient, load-balanced, and scalable molecular simulation. *J. Chem. Theory Comput.* **2008**, *4*, 435−447.
(26) Bonomi, M.; Branduardi, D.; Bussi, G.; Camilloni, C.; Provasi, D.; Raiteri, P.; Donadio, D.; Marinelli, F.; Pietrucci, F.; Broglia, R. A.; Parrinello, M. PLUMED: A portable plugin for free-energy calculations with molecular dynamics. *Comput. Phys. Commun.* **2009**, *180*, 1961−1972.
(27) Sugita, Y.; Okamoto, Y. Replica-exchange molecular dynamics method for protein folding. *Chem. Phys. Lett.* **1999**, *314*, 141−151.
(28) Bonomi, M.; Parrinello, M. Enhanced sampling in the well-tempered ensemble. *Phys. Rev. Lett.* **2010**, *104*, 190601.
(29) Deighan, M.; Bonomi, M.; Pfaendtner, J. Efficient simulation of explicitly solvated proteins in the well-tempered ensemble. *J. Chem. Theory Comput.* **2012**, *8*, 2189−2192.
(30) Essmann, U.; Perera, L.; Berkowitz, M. L.; Darden, T.; Lee, H.; Pedersen, L. G. A smooth particle mesh Ewald method. *J. Chem. Phys.* **1995**, *103*, 8577−8593.
(31) Lifson, S.; Roig, A. On the theory of helixcoil transition in polypeptides. *J. Chem. Phys.* **1961**, *34*, 1963−1974.
(32) Garcia, A. E. Characterization of non-alpha helical conformations in Ala peptides. *Polymer* **2004**, *45*, 669−676.
(33) Best, R. B.; de Sancho, D.; Mittal, J. Residue-specific α-helix propensities from molecular simulation. *Biophys. J.* **2012**, *102*, 1462−1467.
(34) Daura, X.; Gademann, K.; Jaun, B.; Seebach, D.; van Gunsteren, W. F.; Mark, A. E. Peptide folding: when simulation meets experiment. *Angew. Chem., Int. Ed.* **1999**, *38*, 236−240.
(35) Iglesias, J.; Sanchez-Martínez, M.; Crehuet, R. SS-map: Visualizing cooperative secondary structure elements in protein ensembles. *Intrinsically Disord. Proteins* **2013**, *1*, No. e25323.
(36) Kabsch, W.; Sander, C. Dictionary of protein secondary structure: pattern recognition of hydrogen-bonded and geometrical features. *Biopolymers* **1983**, *22*, 2577−2637.
(37) Towse, C.-L.; Hopping, G.; Vulovic, I.; Daggett, V. Nature versus design: the conformational propensities of D-amino acids and the importance of side chain chirality. *Protein Eng., Des. Sel.* **2014**, *27*, 447−455.
(38) Biswas, S.; Sarkar, S.; Pandey, P. R.; Roy, S. Transferability of different classical force fields for right and left handed α-helices constructed from enantiomeric amino acids. *Phys. Chem. Chem. Phys.* **2016**, *18*, 5550−5563.
(39) Sibanda, B. L.; Thornton, J. M. β-Hairpin families in globular proteins. *Nature* **1985**, *316*, 170−174.
(40) Hutchinson, E. G.; Thornton, J. M. A revised set of potentials for β-turn formation in proteins. *Protein Sci.* **1994**, *3*, 2207−2216.
(41) Zerze, G. H.; Uz, B.; Mittal, J. Folding thermodynamics of β-hairpins studied by replica-exchange molecular dynamics simulations. *Proteins: Struct., Funct., Bioinf.* **2015**, *83*, 1307−1315.

DOI: 10.1021/acs.jpcb.8b03157
J. Phys. Chem. B 2018, 122, 6357−6363